

RESEARCH ARTICLE

10.1002/2014JD022600

Key Points:

- El Reno storm produced many large charge moment change (CMC) lightning events
- Positive and negative large-CMC lightnings were related to storm evolution
- Charge moment change has applications to studying tropospheric weather

Correspondence to:

T. J. Lang,
timothy.j.lang@nasa.gov

Citation:

Lang, T. J., S. A. Cummer, D. Petersen, L. Flores-Rivera, W. A. Lyons, D. MacGorman, and W. Beasley (2015), Large charge moment change lightning on 31 May to 1 June 2013, including the El Reno tornadic storm, *J. Geophys. Res. Atmos.*, 120, doi:10.1002/2014JD022600.

Received 18 SEP 2014

Accepted 17 MAR 2015

Accepted article online 23 MAR 2015

Large charge moment change lightning on 31 May to 1 June 2013, including the El Reno tornadic storm

Timothy J. Lang¹, Steven A. Cummer², Danyal Petersen³, Lizxandra Flores-Rivera⁴, Walter A. Lyons⁵, Donald MacGorman⁶, and William Beasley³

¹George C. Marshall Space Flight Center, National Aeronautics and Space Administration, Huntsville, Alabama, USA, ²Department of Electrical and Computer Engineering, Duke University, Durham, North Carolina, USA, ³School of Meteorology, University of Oklahoma, Norman, Oklahoma, USA, ⁴University of Puerto Rico-Mayaguez, Mayaguez, Puerto Rico, ⁵FMA Research, Inc., Fort Collins, Colorado, USA, ⁶National Severe Storms Laboratory, National Oceanic and Atmospheric Administration, Norman, Oklahoma, USA

Abstract On 31 May 2013, a line of severe tornadic thunderstorms (the El Reno event) developed during the local afternoon in central Oklahoma, USA. Within range of the Oklahoma Lightning Mapping Array, the evolution of the event can be separated into three distinct periods: an Early period (before 02:00 UTC on 1 June) when the storm consisted of discrete supercells, a Middle period (02:00–05:00 UTC) when the convection began merging into a linear feature and stratiform precipitation developed, and a Late period (after 05:00 UTC) featuring a mature mesoscale convective system (MCS). Each of these periods demonstrated distinct patterns in the large (>100 C km) charge moment change (CMC) lightning that was produced. During the Early period, large-CMC positive cloud-to-ground (+CG) lightning was produced in the convective cores of supercells. These flashes were small in area (typically <500 km²) and were commonly associated with a sloping midlevel positive charge region in the echo overhang on the storm's forward flank. The Middle period featured a population of larger +CMCs (>500 km², >300 C km) in the developing stratiform, similar to typical sprite-parent lightning in MCSs. During the Late period, convective large CMC +CGs ceased and instead large-CMC negative CGs were produced in and near the MCS convection. These flashes neutralized charge both in convection as well as in adjacent stratiform and anvil precipitation. The results suggest that the CMC metric has potential applications for studying tropospheric weather.

1. Introduction

1.1. Background

Large charge moment change (CMC) lightning has been intimately associated with the production of sprites above thunderstorms [Huang *et al.*, 1999; Hu *et al.*, 2002; Cummer and Lyons, 2005; Lyons *et al.*, 2009; Pasko, 2010; Qin *et al.*, 2012]. This is due to the high electrical stress exerted on the upper atmosphere by the occurrence of hundreds (if not thousands) of C km in charge moment change by powerful cloud-to-ground (CG) lightning strokes in large storms such as mesoscale convective systems (MCSs) [Boccippio *et al.*, 1995; Lyons, 1996, 2006; Lyons *et al.*, 2003; Williams and Yair, 2006; Lyons *et al.*, 2009; Lang *et al.*, 2011]. However, sprite-producing lightning is only a subset of a larger family of rare but powerful lightning that produces large CMCs, and little is known about the meteorology of all flavors of these strokes despite the fact that almost by definition they play a disproportionate role in the global electric circuit [Huang *et al.*, 1999].

Modern capabilities allow the detection and geolocation of large-CMC strokes (hereafter assumed to mean >100 C km, unless otherwise indicated) over the United States [Cummer *et al.*, 2013]. Recent investigations have examined the meteorological context for a subset of these events, known as large impulse CMC (iCMC) strokes, where >100 C km is observed to occur within the first 2 ms of the return stroke [Lang *et al.*, 2013; Beavis *et al.*, 2014]. In storms with normal polarity charge structures (i.e., midlevel negative charge), large-iCMC positive (+) CGs are typically observed to occur in stratiform precipitation regions that are adjacent to strong convection—for example, rearward of the convective line in the commonly occurring leading-line, trailing-stratiform MCS. Most of these flashes initiate as bidirectional breakdown between the midlevel negative and upper positive charge regions in convection and then negative leaders propagate into the stratiform region while gradually descending along known advection pathways for charged ice particles [Lang *et al.*, 2004b; Carey *et al.*, 2005; Ely *et al.*, 2008; Lang and Rutledge, 2008; Lang *et al.*, 2010]. During or after

this time, positive leader branches (possibly starting where negative leaders cut off) come to ground [van der Velde and Montanyà, 2013; van der Velde et al., 2014]. Meanwhile, large-iCMC negative (–) CGs are expected in or near the convective regions and initiate between the upper positive and midlevel negative charge layers. However, instead of negative leaders traveling deep into stratiform precipitation, they remain in or near convection and come to ground close (horizontally) to the initiation point. Overall, a flash associated with a large iCMC –CG ground stroke behaves as a hybrid intracloud (IC)/CG flash and can have a similar structure to a bolt from the blue [Krehbiel et al., 2008; Lu et al., 2012; Lang et al., 2013].

1.2. The El Reno Tornadoic Storm System

On 31 May 2013, a line of severe thunderstorms developed during the local afternoon in central Oklahoma in the United States. One of the supercells produced the El Reno tornado, a large Enhanced Fujita scale 3 [Potter, 2007] multiple vortex tornado that caused significant damage and killed several people, including severe storm researchers Tim and Paul Samaras and Carl Young [Wurman et al., 2014]. After the supercellular stage, the storm system grew upscale into an enormous MCS that affected several states. Much of the storm was in range of the Oklahoma Lightning Mapping Array (OKLMA) [MacGorman et al., 2008] for several hours. During this time, the storm system produced nearly 200 large-iCMC discharges within the 200 km range of the OKLMA. Thus, due to its size, severity, duration, and prolific large-iCMC lightning production, the storm provided an excellent test case for the previously discussed hypotheses describing large-iCMC phenomenology.

2. Data and Methodology

2.1. National Lightning Detection Network

Flash-level CG lightning data from the National Lightning Detection Network (NLDN) were analyzed for the El Reno storm system. This network detects CG lightning in the region of study with an efficiency of >95%, a median location accuracy of <0.5 km, and a report timing of no worse than 1 ms [Cummins et al., 1998; Biagi et al., 2007; Cummins and Murphy, 2009]. Due to the availability of total lightning information from the OKLMA, NLDN intracloud (IC) detections were not considered, except that ICs were counted as CGs if their peak currents were greater than 25 kA. Sensitivity tests were performed with respect to filtering misidentified ICs from the data set by eliminating CGs with low peak currents. Results for both no filtering and a 15 kA filter will be shown.

2.2. Charge Moment Change Network

The Duke University Charge Moment Change Network (CMCN) [Cummer et al., 2013] consists of two distantly spaced (one in Colorado and one in North Carolina) extremely low frequency sensors that measure CMC from CGs that occur within the conterminous United States and surrounding regions. NLDN data are used to geolocate events detected by the CMCN [Cummer et al., 2013], so timing and location uncertainties are similar to those described in the previous subsection. The CMCN data used for this study provided iCMC measurements. This does not include the full continuing current contribution, which can be calculated via laborious postprocessing, and thus provides a lower bound on the total CMC of a CG event. For example, there may be a significant number of +CG flashes with large total charge moment changes which may produce long-delayed sprites [e.g., Lu et al., 2013; van der Velde et al., 2014] but do not attain the threshold of 300 or even 100 C km within the first 2 ms of the stroke. The iCMC magnitude estimates have an uncertainty factor of 1.5 (i.e., +50%/–33% [Cummer et al., 2013]). The use of iCMC measurements in lightning research has an established history [Huang et al., 1999; Cummer and Inan, 2000; Cummer and Lyons, 2004, 2005], and recent studies [Cummer et al., 2013; Lang et al., 2013; Beavis et al., 2014] have begun documenting the additional meteorological and climatological information provided by them. In terms of the impacts on transient luminous event (TLE) production, CGs with iCMCs ~100 C km have an approximately ~10% chance to produce a sprite, while iCMCs ~300 C km are 75–80% likely to produce a sprite [Lyons et al., 2009]. This latter category is herein termed “sprite-class” iCMCs, following Beavis et al. [2014].

2.3. Oklahoma Lightning Mapping Array

The Oklahoma Lightning Mapping Array (OKLMA) [MacGorman et al., 2008] locates very high frequency (VHF) bursts from lightning, enabling mapping of flashes in three-dimensional (3-D) space plus time. Postprocessed, full-rate data (i.e., not decimated real-time data) were analyzed in this study. The timing and spatial uncertainties associated with the data from LMAs in general, as well as from the OKLMA in particular, have been documented by several studies [e.g., Koshak et al., 2004; Thomas et al., 2004; MacGorman et al., 2008;

Lang et al., 2010]. The parameter most critically affected by range from network center is vertical uncertainty in individual sources, which for the OKLMA is approximately 0.9 km at 100 km range and 2.1 km at 200 km range (for location solutions with chi-square error ≤ 1 [Lang et al., 2010]). However, as Lang et al. [2010] demonstrated, the uncertainty for the mean vertical positions of groups of sources at long distances is much less than this, <0.5 –1 km. Thus, long-range OKLMA data (100–200 km) are still useful for determining the mean vertical positions of flashes. Lang et al. [2010] also showed that upward bias in vertical source locations at long ranges [Thomas et al., 2004] is not a major concern for the region within 200 km of OKLMA.

flash In order to limit the effects of the decline of OKLMA detection efficiency with increasing range [Lang et al., 2011], only storms within at most 200 km of the OKLMA centroid were examined. Automated flash identification and counting was done using the XLMA software developed at the New Mexico Institute of Mining and Technology, similar to the methodology of Lang and Rutledge [2008]. Specifically, 10 VHF sources were required to count a flash via automated algorithm, and each source must have been detected by at least 7 OKLMA stations and located with a chi-square error ≤ 1 . Sensitivity tests that lowered the source number requirement from 10 to 5 were performed, and these results also will be shown. The total number of active OKLMA stations during the El Reno storm was 12 before 01:50 UTC on 1 June (with one exception discussed later) and 11 thereafter. Flash areas were computed using the area of the convex hull surrounding all plan-projected sources in a flash, similar to Bruning and MacGorman [2013]. In the time series of characteristics that were produced, analysis focus was placed on interpreting trends versus absolute magnitudes.

In order to improve the accuracy of OKLMA-mapped characteristics for the flashes of most interest in this study (i.e., those associated with large and sprite-class iCMCs), these individual flashes were also isolated by hand using XLMA, following Lang et al. [2010, 2011]. This hand analysis was done for flashes with iCMC > 100 C km within 120 km of OKLMA. In addition, the individual structure of flashes producing sprite-class iCMCs (>300 C km) was also hand analyzed even if they were in the 120–200 km range, as these flashes tended to be larger and more isolated in space and time. This made them well resolved by OKLMA despite the degraded detection efficiency and vertical resolution and enabled a significant increase in the number of available sprite-class iCMC flashes for analysis. During this manual processing, the relative locations of LMA-mapped positive and negative charge regions associated with each flash were noted.

2.4. Multiradar/Multisensor National Radar Mosaics

The National Oceanic and Atmospheric Administration (NOAA) regularly produces the multiradar/multisensor (MRMS) 3-D radar reflectivity mosaics (formerly the National Mosaic and Multisensor Quantitative Precipitation Estimation, or NMQ, mosaics) covering the entire conterminous United States [Zhang et al., 2011]. During May/June 2013, these mosaics were available every 5 min as eight separate regional tiles. The horizontal spatial resolution was 0.01° in latitude and longitude. The vertical coordinate contained 31 levels and ranged from 0.5 km above mean sea level (msl) up to 18 km, with spacing of 0.25 km near the surface gradually stretching to 2 km aloft.

At the National Aeronautics and Space Administration (NASA) George C. Marshall Space Flight Center, an open-source, object-oriented software package has been developed in the Python language to read MRMS mosaics into a common data structure, to visualize the reflectivity structure of storms, and to enable quantitative analysis. The software package, titled the Marshall MRMS Mosaic Python Toolkit (MMM-Py), also performs the data array stitching needed when large storms (like El Reno) cross regional tile boundaries. MMM-Py was used for production of nearly all radar analyses and radar figures used in this study. The only exceptions were the time series of reflectivity volumes, which were calculated prior to MMM-Py development using older software written in the Interactive Data Language (IDL) following Lang et al. [2013].

3. Results

3.1. Case Overview

Basic CG lightning statistics for the El Reno storm are shown in Table 1. With no thresholding of the NLDN data, the storm was strongly $-$ CG dominant. However, removing small-peak-current negative discharges from the CG data set led to a nearly fourfold reduction in $-$ CG flash counts. The $+$ CG data set was unaffected as it was evidently already prefiltered for weak discharges by Vaisala. The overall storm in the range of OKLMA was still $-$ CG dominant in the filtered data, but the ratio was less than 2:1. Combined radar and lightning

Table 1. Cloud-to-Ground (CG) Lightning Totals for the El Reno Storm System (20:00 UTC, 5/31 Through 10:00 UTC, 6/1) for Various Ranges From the OKLMA Centroid

	+CGs	−CGs
All CGs (<200 km)	6,453	42,283
All CGs (<200 km; 15 kA threshold)	6,453	11,026
iCMC > 100 C km (<200 km)	101	98
iCMC > 100 C km (<120 km)	55	18
iCMC > 300 C km (<200 km)	17	14

analysis focused on a subset of the period from 20:00 UTC on 31 May 2013 (before the initiation of any cells) to 12:00 UTC the next day (late in the MCS stage of the event, when it was exiting Oklahoma). Figure 1 shows an hour each of large-iCMC strokes overlaid on eight representative radar mosaics from that time period. The discrete

cell/supercell stage (roughly 22:00–02:00 UTC) included the time period during which the main supercell (the core near the center of the OKLMA network in Figures 1b and 1c) produced the tornado (23:03–23:43 UTC). There are a number of large-iCMC +CGs (>100 C km), almost all apparently associated with the convective portion of the tornadic supercell, in the 23:00 and 01:00 UTC plots (Figures 1b and 1c). Nearly all of these occurred near the center of the OKLMA. During this time, there were very few large-iCMC −CGs within 200 km of the OKLMA.

Many hours later (e.g., 07:00 and 09:00 UTC; Figures 1f and 1g), the situation had changed. The storm system had grown upscale into a large MCS. Convection along an east-west oriented line hosted a large number of large-iCMC −CGs, while most large-iCMC +CGs were found to the north in stratiform precipitation, almost all of which were unfortunately out of range of the OKLMA. However, during the transition period between these two storm structure paradigms (e.g., 03:00 and 05:00 UTC; Figures 1d and 1e), some large-iCMC +CGs did occur within range of the OKLMA, in a region of stratiform precipitation (where reflectivities were below 40 dBZ) 100–200 km northeast of the OKLMA center, and many of the stratiform large-iCMC +CGs were sprite class (>300 C km). There were also a few convective large-iCMC +CGs.

The remainder of this paper will focus mainly on large-iCMC lightning and other storm metrics within at most 200 km of the OKLMA. This enables the inclusion of OKLMA data in the analyses.

3.2. Time Series Analysis

Time series for radar and lightning data are shown in Figure 2. In general, both OKLMA total lightning (10-source requirement; Spearman’s rank correlation coefficient = 0.81) and unfiltered NLDN total CG lightning (correlation = 0.91) were well correlated with 40 dBZ radar echo volume (Figure 2a). However, reducing the LMA source requirement to 5 improved the correlation with 40 dBZ echo volume to 0.87, and the improvement was most evident during approximately 22:00–06:00 UTC. Subjecting total CGs to a 15 kA filter, however, greatly reduced the correlation with 40 dBZ reflectivity to 0.51. All of the above correlations were statistically significant at a level greater than 99%. This variability in the time series, depending on threshold, suggests that small and weak IC flashes, many of which were likely misidentified by the NLDN as −CGs, disproportionately occurred during the earlier stages of the storm. Interestingly, there was a sharp reduction in total lightning immediately prior to the start of the tornado, a phenomenon that has been observed in other storms as well [e.g., Williams *et al.*, 1999].

Figure 2b demonstrates that with no filtering, the storm system appeared to be dominated by −CG lightning overall. However, filtering on peak current removed this dominance, and prior to 02:00 UTC, the relative +CG/−CG fractions were close to even (2427 filtered −CGs to 2650 +CGs), and −CG dominance did not occur until afterward. In fact, between 00:30 and 01:00 UTC, the storm was +CG dominant according to the filtered NLDN time series. Large-iCMC lightning was split nearly evenly between the two polarities (Table 1). However, these showed an interesting binary behavior, with large-iCMC +CGs favored earlier than large-iCMC −CGs (Figure 2b). With both polarities, however, the >300 C km CGs began to occur only after several hours of >100 C km activity.

The OKLMA data were investigated in more detail in order to better understand the reasons for this large-iCMC behavior. Within 120 km of the OKLMA centroid, the storm can be subjectively split into two periods before and after ~04:45–05:00 UTC. Prior to that time, the mode of OKLMA source density remained mostly below 10 km above mean sea level (msl) (Figure 3a), and when the storm produced large-iCMC CGs, they were mostly positive. After this time, the OKLMA source density mode lifted above 10 km, and the storm began to produce almost exclusively large-iCMC −CGs (within 120 km of the OKLMA). In addition to

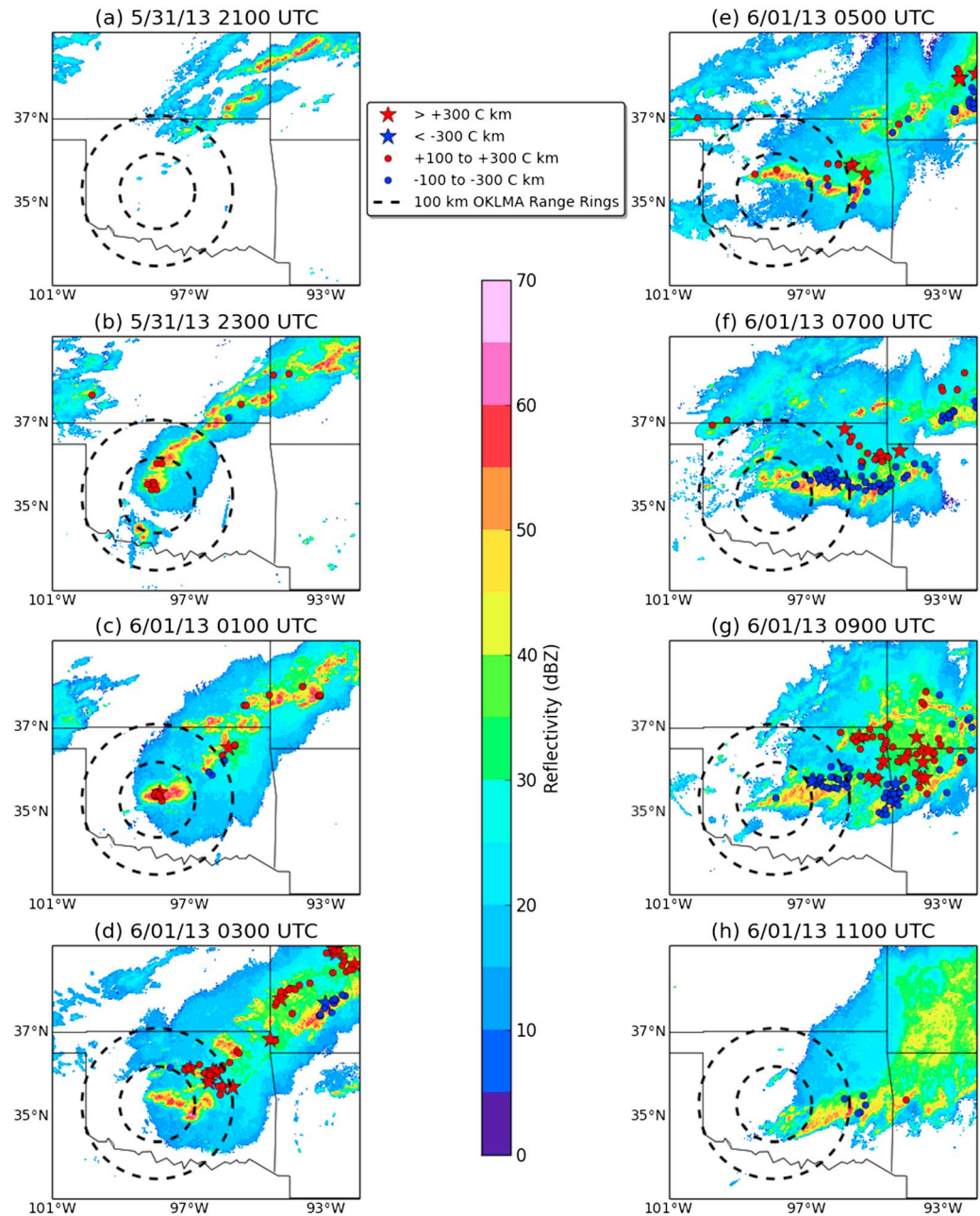


Figure 1. Two hourly updates of composite radar imagery and large-iCMC lightning from 21:00 UTC on 31 May 2013 to 11:00 UTC on 1 June. One hour of lightning surrounding each indicated time is displayed. U.S. state boundaries and OKLMA range rings are also shown.

flash rate, VHF source density also declined during the tornado. Flash areas are displayed alongside OKLMA flash rate in Figure 3b. Often flash rate and median flash area evolved in a quasi-anticorrelated manner (although actual correlations were low and not statistically significant at the 99% level), and the post-04:45 UTC period was dominated by fewer but larger flashes compared to pre-04:45 UTC.

The median altitudes and convex hull areas of OKLMA sources associated with strokes featuring iCMC > 100 C km are shown in Figure 4, which only focuses on flashes within 120 km from OKLMA. These metrics mainly provide information on the behavior of negative leaders in each flash [Rison *et al.*, 1999]. The differences in altitude between the +CGs and the -CGs (Figure 4a) are striking. The OKLMA-mapped altitudes

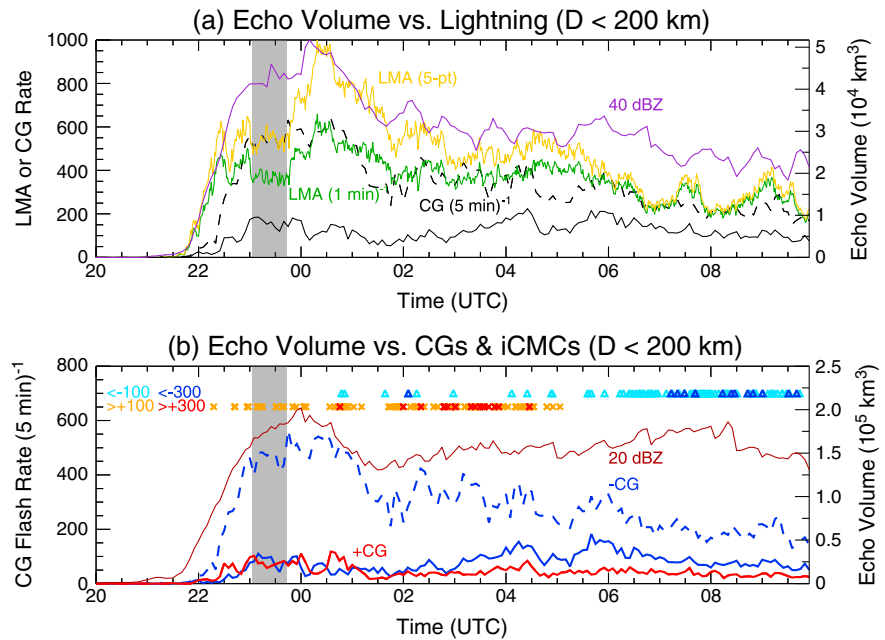


Figure 2. (a) Time series of 40 dBZ echo volume (purple), total CG flash rate (black; solid:15 kA filter, dash: no filter), and OKLMA total lightning flash rate (green: 10-source minimum, yellow: 5-source) within 200 km of the OKLMA center. The gray shaded region is the time of the El Reno tornado. (b) Similar to Figure 2a but showing positive (red) and negative (blue) CG time series, as well as 20 dBZ echo volume (brown). Solid CG time series curves use a 15 kA filter, while dashed curve is for no filter (+CG curves are virtually identical and thus overlap). The times of large-iCMC strokes, broken out by 100 and 300 C km thresholds, are indicated above the time series.

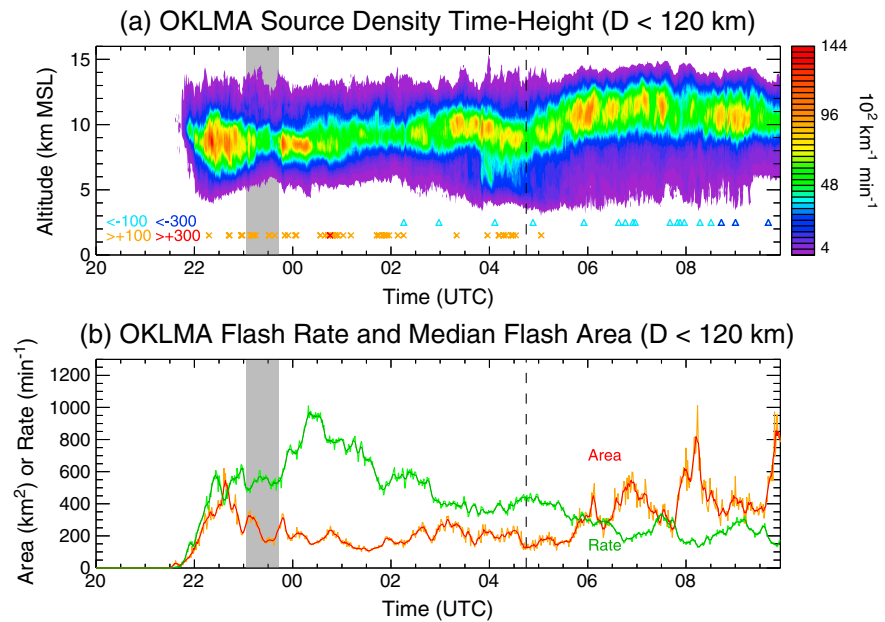


Figure 3. (a) Time-height contour plot of VHF source density from the OKLMA for the portions of the El Reno storm system within 120 km of the network. Also shown are the large-iCMC event times similar to Figure 2b but for the adjusted range criterion. (b) Time series of OKLMA median flash area (red) and total flash rate (green). The threshold is minimum 5 points per flash. The lighter curves are 1 min resolution, while the darker curves are 5 min running means. The time of the El Reno tornado is shown by the gray shaded region in each subplot. The vertical dashed line is used to subjectively indicate where a significant change in lightning behavior began to occur.

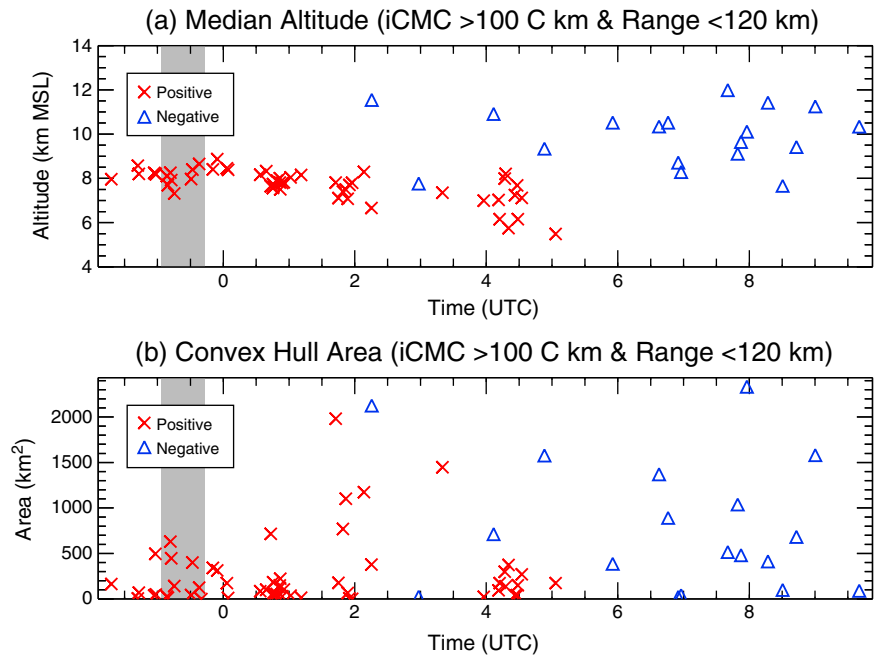


Figure 4. (a) Times and median altitudes of large-iCMC strokes. Thresholds were 100 C km iCMC and 120 km distance from OKLMA. El Reno tornado time is shaded. (b) Similar to Figure 4a but for convex hull area of each flash.

of large-iCMC +CGs rarely exceeded 8 km msl on average, while for –CGs, the vertical range was 8–12 km. While large-iCMC +CGs (Figure 4b) sometimes featured large areas (>500 km²), this was not the rule, and the relative fraction of large-iCMC –CGs above that threshold was much greater. The tendency for small-area, large-iCMC +CGs does not match the model of a large-CMC or sprite-parent +CG starting as negative leaders propagating tens to hundreds of kilometers into stratiform precipitation, while a positive leader comes to ground either in convection or stratiform precipitation [Lang et al., 2010; van der Velde et al., 2014].

The sprite-class events were examined in a similar manner (Figure 5). As mentioned before, due to the small number of these flashes (Table 1), the OKLMA range criterion was extended to 200 km. Both flash polarities featured similarly large convex hull areas for sprite-class events. With the exception of one negative event at 02:05 UTC, the different sprite-class iCMC polarities occurred during distinct time periods: ~02:00–04:00 UTC for sprite-class +CGs and 07:00–10:00 UTC for sprite-class –CGs. This is in agreement with Lang et al. [2013], who found that coincident or collocated sprite-class positive and negative events were rare. However, this excludes the region beyond 200 km, which produced multiple sprite-class positives and negatives during the latter 07:00–10:00 UTC time period, although these were not collocated (Figures 1f and 1g).

Negative sprite-class flashes still maintained a higher altitude than the sprite-class positives (Figure 5a), although the latter were higher in altitude than the >100 C km +CGs (Figure 4a), with several above 9 km msl. As discussed in section 2.3, this is not explainable just by network effects and the range criterion relaxation between Figures 4 and 5. Since LMAs are most sensitive to negative breakdown within positive charge layers [Rison et al., 1999], this suggests that the positive charge layer neutralized by the sprite-class discharges was somewhat higher (1–2 km) on average than for the smaller iCMC discharges. Since the latter occurred mostly in convection and the former in stratiform precipitation (Figure 1), this altitude difference is explainable in terms of storm structure, as will be demonstrated in the next section. For both large- and sprite-class iCMCs, specific iCMC values were not correlated with either parent-flash altitude or area.

Figure 6 shows the percentage of each large-iCMC flash’s area containing composite reflectivity >40 dBZ, as a function of time. Flashes that were mainly in convective regions should have a high value for this parameter (>50%), while those in mainly stratiform precipitation should have the opposite. For large iCMCs within 120 km of the OKLMA (Figure 6a), the positive events were mainly >50% except for the 01:30–04:00 UTC time period when both large-iCMC and sprite-class positives (Figure 6b) contained very little echo >40 dBZ within

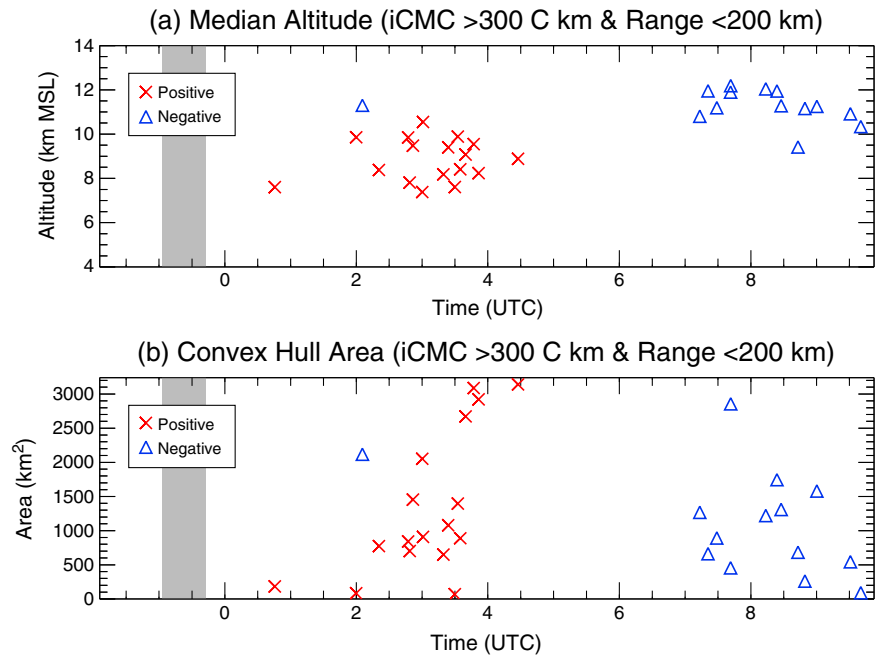


Figure 5. Same as Figure 4 but now the thresholds are iCMC > 300 C km and OKLMA distance < 200 km.

their respective OKLMA-mapped parent flash areas. These latter flashes typically occurred in stratiform precipitation, a fact that was confirmed during investigation of individual flashes (see next section). By contrast, both the large-iCMC and sprite-class negatives occurred in a mixture of >40 dBZ percentages, indicating no specific preference for stratiform versus convective locations. As will be illustrated by an

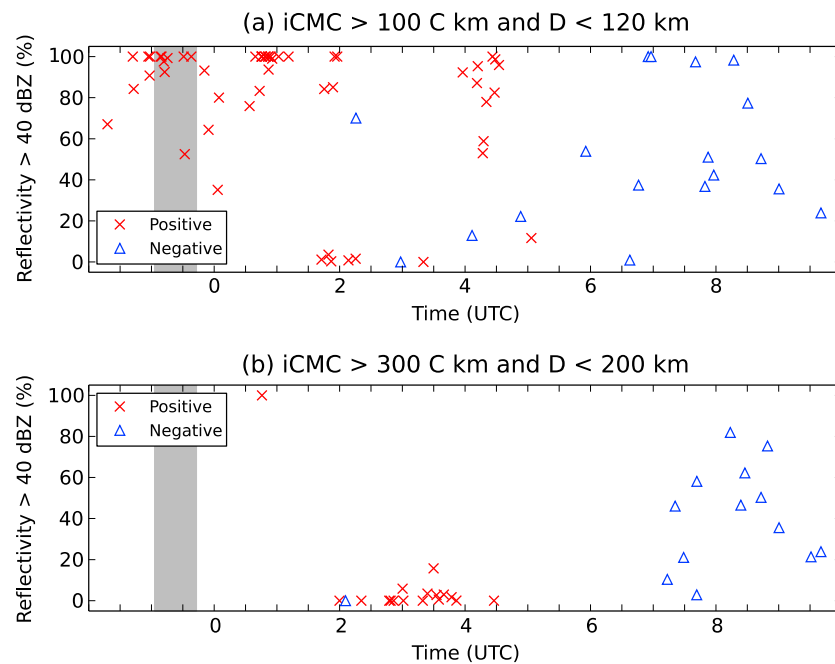


Figure 6. (a) Times and percentages occurring within MRMS composite reflectivity >40 dBZ for OKLMA-mapped large-iCMC flashes, as estimated via two-dimensional flash convex hulls. The thresholds were iCMC > 100 C km and OKLMA range < 120 km. The El Reno tornado time is shaded gray. (b) Similar to Figure 6a but for iCMC > 300 C km and OKLMA range < 200 km.

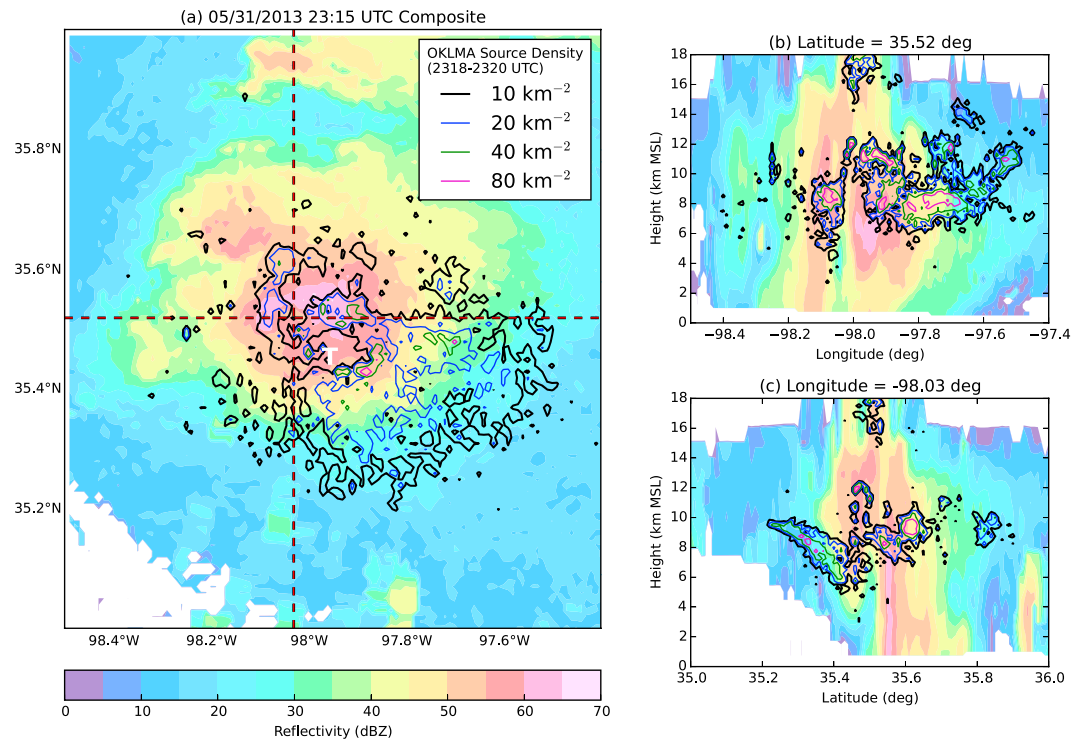


Figure 7. (a) Plan view of composite radar reflectivity at 23:15 UTC focusing on the El Reno supercell during its tornadic stage. (b) Similar to Figure 7a but now a vertical cross section through the indicated constant latitude. OKLMA data are from within $\pm 0.05^\circ$ latitude of the cross section. (c) Similar to Figure 7b but for the indicated constant longitude. Also shown are the line contours of plan-projected OKLMA source density from the period of 23:18 to 23:20 UTC. The red dashed crosshairs indicate the vertical cross sections in Figures 7b and 7c. The white *T* indicates the approximate center of the El Reno tornado at 23:18 UTC (via <http://maps.google.com>).

example in the next section, these negative iCMCs typically occurred near the edges of large convective precipitation cores, with access to adjacent stratiform precipitation regions.

3.3. Radar and Flash Structure

Although this study was mainly focused on large-CMC lightning, the reductions in total flash rate and LMA source density (Figures 2 and 3) during the tornado demand some attention. During a portion of the 23:03–23:43 UTC tornadic time period, the West Minco OKLMA station (35.362°N , 98.040°W , near the main supercell) stopped reporting any sources despite being listed as an active station. However, this outage did not completely overlap the tornado's lifetime (it was most significant during 23:20–23:40 UTC), and a reduction in detected VHF sources was observed across all active stations during the tornado. Adjustments to the number of stations required to locate a source (e.g., varying the criterion between as few as 1 station and as many as 10 stations) did not affect the results during this time period. Thus, this lightning reduction is not explainable simply in terms of network effects.

Further inspection of combined MRMS and OKLMA data indicated that a lightning hole associated with strong updrafts [Krehbiel et al., 2000; Lang et al., 2004a; Goodman et al., 2005] was a possible cause of this lightning reduction (Figure 7). Indeed, the behavior of the lightning appears to have been strongly affected by the mesocyclonic/tornadic circulations in the storm [Wurman et al., 2014], with spiral band-like structures in the plan-projected LMA source densities in the storm's core (Figure 7a). Vertical cross sections through this core (Figures 7b and 7c) show a nearly lightning-free region associated (if not entirely collocated) with a bounded weak-echo structure in the radar data. There was also substantial lightning activity at extremely high altitudes, in the overshooting top of the thunderstorm (>16 km msl). This high-altitude activity is commonly observed in strong thunderstorms and supercells [Krehbiel et al., 2000; MacGorman et al., 2008; Bruning et al., 2010; Emersic et al., 2011; Meyer et al., 2013].

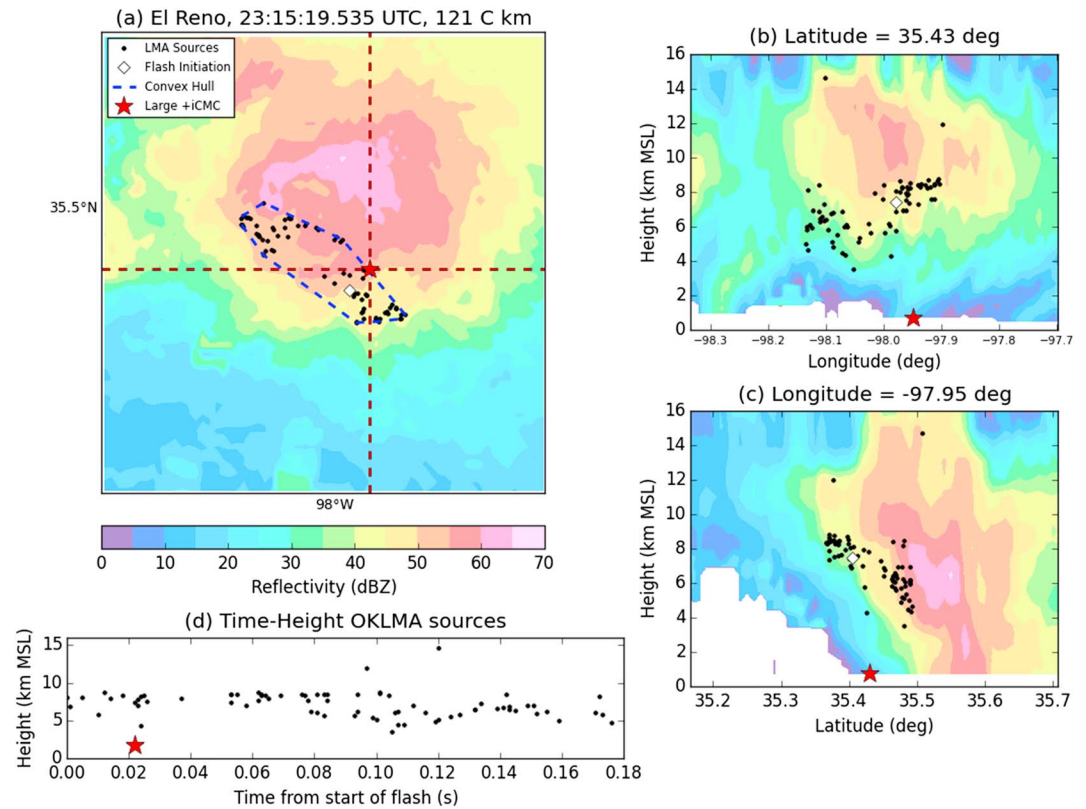


Figure 8. Typical example of a large-iCMC +CG (121 C km) during the early supercell stage of the El Reno storm system. The flash occurred at the indicated time, with radar data coming from 23:15 UTC. (a) Plan view with composite radar reflectivity (filled contours) and lightning data indicated according to the legend. (b) Vertical cross section through the indicated constant latitude. (c) Same as Figure 8b but for the indicated constant longitude. (d) Time-height plot of LMA sources and large-iCMC stroke timing during the flash. The red dashed crosshairs indicate the vertical cross sections in Figures 8b and 8c.

The lightning reduction may also have been related to the production of wet-growth hail during this time period [Emersic et al., 2011]. As noted by that study, wet-growth hail suppresses rebounding during collisions with cloud ice and thus can inhibit charge separation.

These meteorological hypotheses to explain the lightning reduction deserve further testing via analysis of multiple Doppler and polarimetric radar data from this time period, but that is beyond the scope of the present study. For the purposes of the current work, it is enough to note the existence of the lightning reduction and establish that it is likely a real meteorological effect and not due to OKLMA network issues.

Note the vertically slanted lightning structure in the echo overhang associated with the forward flank precipitation [Browning, 1964] (between 35.2° and 35.4° latitude; Figure 7c). This region was the primary generator for large-iCMC +CGs during the early lifetime of the El Reno storm system (22:00–02:00 UTC). A typical example of a large-iCMC +CG during this discrete cellular/supercellular stage were found to occur along the edges of convective cores. Initiation was near midlevels (~8 km), and lateral propagation was minimal (<10 km) before striking ground. In many of these +CGs, sloped reflectivity structures (Figure 8c) were associated with the echo overhang (similar to the sloping in the lightning source densities in Figure 7c). Meanwhile, CGs in the high-reflectivity core of the storm (not shown) were primarily negative (Figure 2b); however, the use of 15 ka filtering reduced those numbers considerably as previously noted.

As seen in Figure 5, the 02:00–04:00 UTC period was an active period for the production of large and sprite-class positive iCMCs in stratiform echo that developed to the northeast of the convection that was located near the center of the OKLMA network. A typical example of these flashes is shown in Figure 9. This

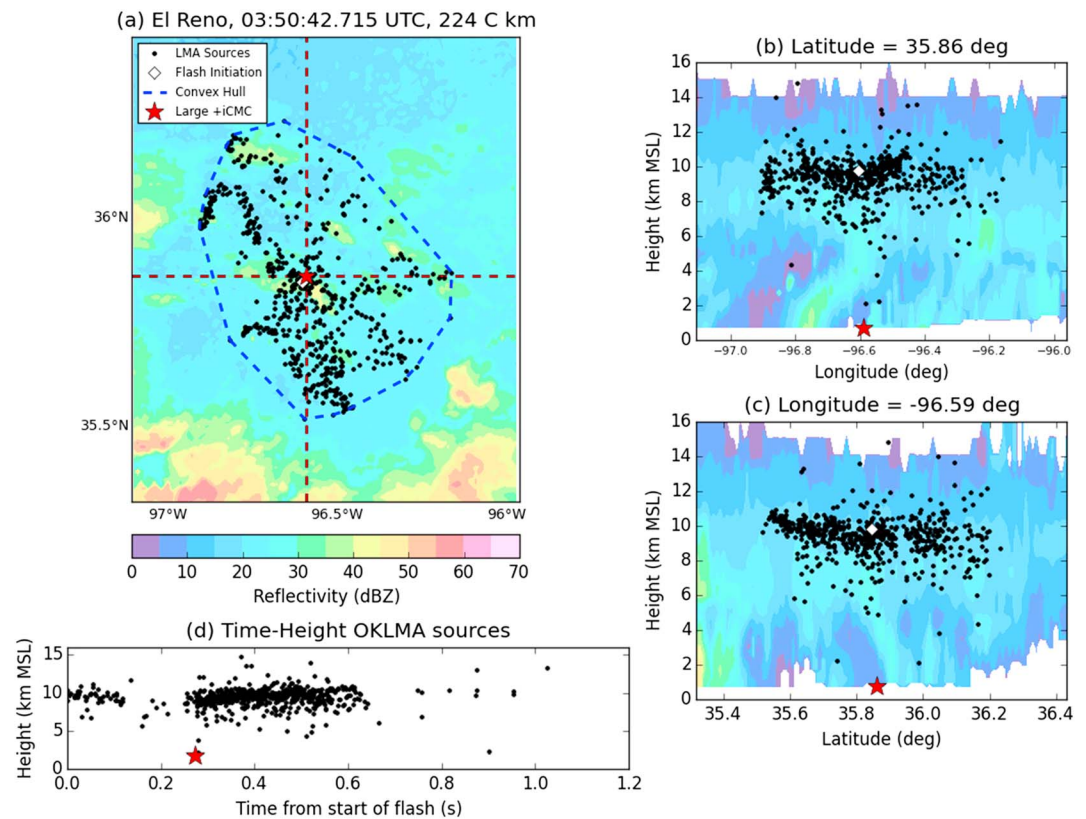


Figure 9. Same as Figure 8 but now for a typical large-iCMC +CG (+224 C km) in the stratiform region of the El Reno storm system during its later mesoscale stage. The radar data are from 03:50 UTC.

particular flash occurred around 03:50 UTC beyond 100 km from the OKLMA centroid. Due to this distance, detailed mapping of low-altitude flash behavior is not expected, and overall 3-D structure of the flash would be expected to be only coarsely resolved [Thomas et al., 2004; MacGorman et al., 2008; Lang et al., 2010, 2011]. Nevertheless, some key features are visible. Specifically, the flash initiated and struck ground near the same horizontal position and the in-cloud lightning spread out horizontally from that point in a dendritic manner (Figure 9a). The reflectivity structure was mostly stratiform here, with some indications of weak/decaying embedded convection, which may have enhanced local charging of the cloud. OKLMA sources were clustered near 9–11 km msl, suggesting that upper level positive charge was being neutralized by this flash. In fact, the stratiform large-iCMC +CGs during this time period were clearly involving a higher positive charge layer than the convective large-iCMC +CGs observed during the discrete cellular/supercellular stage (Figure 8).

A large-iCMC –CG that featured near-average geometry (e.g., area was 1582 km² and median altitude was 11.2 km msl) is shown in Figure 10. Large-iCMC –CGs were much larger than their convective +CG counterparts, despite still occurring in—or on the periphery of—convection. The high median altitudes for these flashes are explained by individual flash behavior, which demonstrated a bilevel structure very similar to IC flashes, with upper level positive charge near 10–12 km msl and midlevel negative charge near 6–8 km msl (Figures 10b and 10c). These flashes typically then struck ground late in their development, when middle and lower level LMA sources were mostly occurring (e.g., Figure 10d). This hybrid IC/CG behavior in large-iCMC –CGs is very common [Lu et al., 2012; Lang et al., 2013].

4. Discussion

The behavior of large-CMC lightning clearly reflected the evolution of the El Reno storm system. The three major stages of the storm—the Early period (<02:00 UTC on 1 June) containing discrete cells and supercells, the Middle period (02:00–05:00 UTC) featuring the development of a linear storm system and the formation

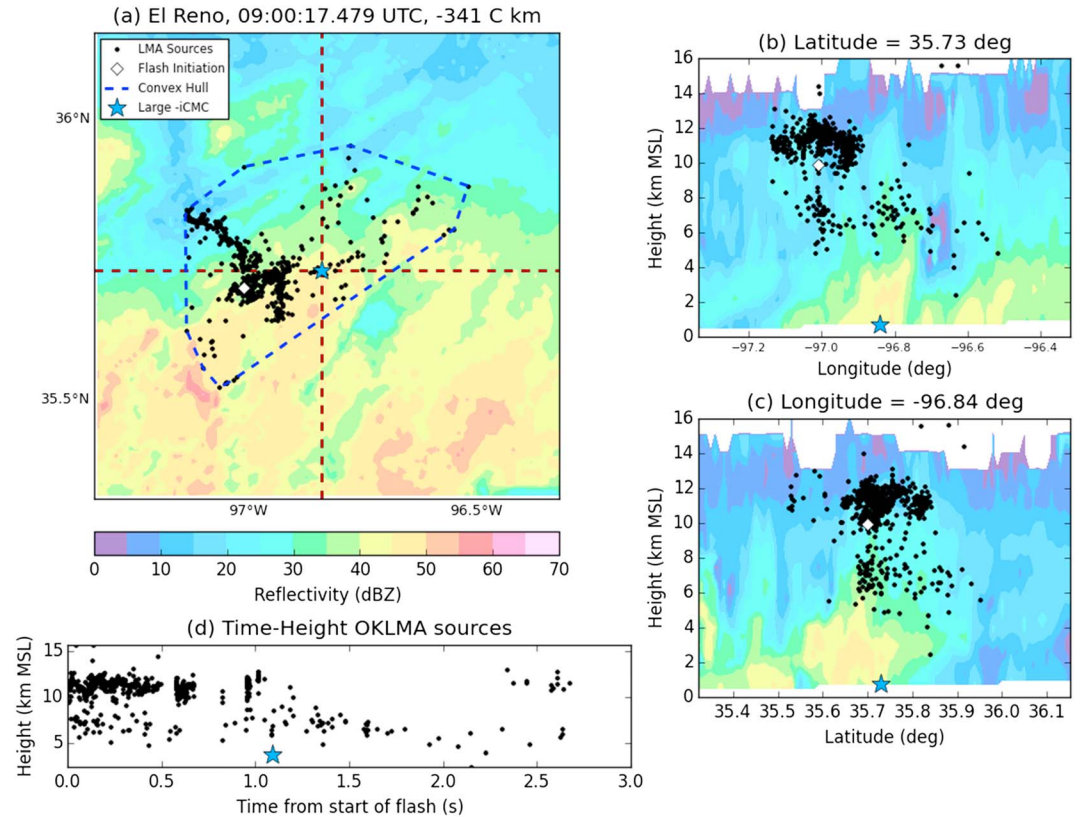


Figure 10. Same as Figure 8 but now for a typical large-iCMC -CG (-341 C km). The radar data are from 09:00 UTC.

of a significant region of stratiform precipitation, and the Late period (>05:00 UTC) featuring an organized MCS—all featured distinct large-CMC characteristics.

4.1. Early Period (<02:00 UTC)

During the Early period, the El Reno storm system featured VHF lightning source densities that were maximized near 8–9 km msl. However, particularly during the tornado, complex lightning structures featuring significant horizontal heterogeneity existed. Of key interest was a sloping positive charge region near midlevels, on the outskirts of strong convection and within the echo overhang on the forward flank of the storm (Figure 7). This structure was the source of multiple large-iCMC +CGs during the early lifetime of this storm system. The VHF sources in these convective large-iCMC +CGs covered relatively small areas and demonstrated very little lateral propagation before (or after) the positive leader came to ground.

While unfiltered CG data suggested -CG dominance during the early stage, filtered data told a different story, that the ratio of -CGs and +CGs was close to 1:1. A storm producing >50% +CGs is typically an indication of it having an anomalous charge structure [Carey and Rutledge, 1998; Williams, 2001; Lang et al., 2004a; Wiens et al., 2005; Lang and Rutledge, 2011; Bruning et al., 2010, 2014]. Great Plains supercell charge structures are known to be complex [Stolzenburg et al., 1998; Wiens et al., 2005; Bruning et al., 2010], and El Reno’s lightning behavior (e.g., Figure 7) also suggests a complex charge structure. Manual inspection of individual LMA flashes demonstrated the existence of numerous small-scale IC flashes during this period, and the flash size statistics (Figure 3b) supported this observation, particularly during 23:00–02:00 UTC. This likely indicated the effect of turbulent eddies on limiting flash sizes near the thunderstorm’s updraft region [Bruning and MacGorman, 2013]. Manual inspection of KTLX (Oklahoma City) radar data during the 23:00 UTC hour confirmed the existence of large spectrum width values (5–15 m s⁻¹ and higher) within the tornadic storm core, indicating strong turbulence [Istok and Doviak, 1986]. The small sizes of the large-iCMC +CGs that occurred during this time period thus are best understood within this context.

During the Early period, the El Reno tornado occurred shortly after 23:00 UTC following a rapid increase in storm echo volumes and total flash rate (from near zero to $400\text{--}600\text{ min}^{-1}$ depending on source threshold) during 21:45–22:30 UTC (i.e., a “lightning jump”) [Williams *et al.*, 1999; Schultz *et al.*, 2009, 2011; Darden *et al.*, 2010; Gatlin and Goodman, 2010]. Large-iCMC +CGs started occurring after 22:00 UTC. Immediately prior to the actual tornado, the OKLMA recorded a $\sim 100\text{ min}^{-1}$ reduction in total flash rate, which appeared to be related to the lightning hole and other complex lightning structures evidently caused by the tornadic and mesocyclonic circulations (e.g., spiral arms in Figure 7) that formed during this time period. Wet growth of hail may also have played a role. The OKLMA flash rate rapidly recovered after the tornado lifted, with total flash rate within 200 km of OKLMA peaking during 00:00–00:30 UTC. The 40 dBZ echo volume peaked shortly after 00:00 UTC and then rapidly declined until 01:00 UTC when it started declining more slowly. This behavior reflected the growth, maturity, and decay of the tornadic supercellular stage of the El Reno storm.

4.2. Middle Period (02:00–05:00 UTC)

Small, convective large-iCMC +CGs were also favored during the 04:00–05:00 UTC time period, in the western edge of the convective line that was developing (e.g., Figure 1e). Inspection of the OKLMA data suggested similar flash behavior to the pre-02:00 UTC time period, with large-iCMC +CGs favored near the edges of convection. The LMA source density lowered in altitude (Figure 3a) during this time, suggesting that another anomalous charge structure had developed in the new convection at the western edge of the line [Lang and Rutledge, 2011]. Manual inspection of the OKLMA data confirmed this inference. Based on flash behavior, all of the convective large-iCMC +CGs during the Early and Middle periods appear to be akin to the sprite-class +CGs in mature supercells studied by Lyons *et al.* [2008]. That is, the LMA-mapped flashes were short lived ($\sim 200\text{ ms}$ or less), not laterally extensive ($< 500\text{ km}^2$), and the ground strokes were largely impulsive events, where the return stroke likely accounted for most of the charge transfer, and very little continuing current would have been observed.

By contrast, during part of the Middle period (02:00–04:00 UTC), most of the large-iCMC +CGs were larger in terms of both area and magnitude (i.e., were more likely to be sprite class, $> 300\text{ C km}$). They all initiated outside of strong convection ($> 40\text{ dBZ}$), and their LMA sources were confined to regions of mostly stratiform echo. They occurred 1–2 km higher in altitude than convective large-iCMC +CGs. This period occurred as the storm was transitioning from primarily a series of discrete cells and supercells to a linear system with a significant amount of stratiform precipitation. These stratiform +CGs persisted into the 04:00–05:00 UTC hour during this middle period but do not show up well in the time series as many were out of range of OKLMA. During this middle/transition period, 40 dBZ echo volumes declined overall, while 20 dBZ echo volumes recovered and began increasing from the relative minimum observed during 01:00–02:00 UTC. This indicated a transition from strong convection in the Early period to a more widespread mesoscale precipitation system with a significant amount of stratiform echo. This overall structure is very conducive to the production of large-iCMC +CGs and sprite-class/sprite-parent +CGs in stratiform precipitation, as documented extensively by past studies [Boccippio *et al.*, 1995; Lyons, 1996, 2006; Lyons *et al.*, 2003; São Sabbas and Sentman, 2003; Williams and Yair, 2006; Lang *et al.*, 2010; Soula *et al.*, 2009, 2014], and El Reno was no different.

4.3. Late Period ($> 05:00\text{ UTC}$)

Around 05:00 UTC, a significant change in the convection occurred. By this storm, the storm was a mature MCS. There was a resurgence in 40 dBZ echo volumes, but this only briefly arrested the long-term secular decline as the storm moved out of OKLMA range. However, this resurgence was associated with an increase in the altitude of the OKLMA source maximum to roughly 10–11 km msl (Figure 3a). This marked the transition to the third stage of the El Reno storm, from OKLMA's perspective. At this point, the storm went from only intermittently producing large-iCMC –CGs to producing them much more frequently in and near convection. Stratiform large-iCMC +CGs continued, but they were mainly out of OKLMA range after 05:00 UTC. Since the storm grew upscale with time, this suggests the effects of the lateral growth of charge layers in both convective and stratiform regions. Combined with the likely higher altitudes for charge layers, as inferred from the OKLMA source density behavior (e.g., Figure 3a), this suggests an increase in both the charge (Q) and the altitude (Z) terms of the CMC equation (i.e., $\text{CMC} = Q \times Z$) [Lang *et al.*, 2011], making it more likely for the most powerful –CGs to exceed the iCMC thresholds used in this study. Inspection of individual large-iCMC –CG flashes during this time period (e.g., Figure 10) found that they were initiating between upper level positive charge and midlevel negative charge. This suggests the existence of a more conventional

normal polarity charge structure [Krehbiel *et al.*, 2008], which would be consistent with the higher LMA modal altitude observed during this time [Lang and Rutledge, 2011].

The linear structure of the convection in the late-stage El Reno storm roughly matches the basic character of the convection that produced most of the large-iCMCs and negative sprite parents studied by Lang *et al.* [2013], that is, a large area of strong, contiguous, multicellular convection. However, as that study mostly lacked LMA information, the present study brings a new insight: the importance of the adjacent stratiform and anvil precipitation regions for large-iCMC –CGs, as both high- and lower-altitude LMA sources often extended into weak (<40 dBZ) reflectivities (e.g., Figures 6 and 10). These regions evidently provided access to a larger, more extensive negative charge layers that were not being neutralized regularly by frequent lightning flashes in the thunderstorm core(s).

5. Conclusions

Due to its public impacts, its longevity, and its high production of large-CMC lightning in range of an LMA, the El Reno storm was an excellent case for studying the phenomenology and meteorology of large-CMC lightning. This lightning comprises a small subset of the total population of CGs, but its impacts on thunderstorm charge and the global electrical circuit (including the production of sprites, halos, and elves) are disproportionately large. As seen in the El Reno storm, and similar to what has been observed in other storms [Lang *et al.*, 2013], the positive and negative versions of this lightning are generally not collocated. In addition, this study clearly demonstrates that the behavior of large-CMC lightning can reflect the evolution of storms, from discrete cells and supercells to upscale growth into a mature MCS. While the results of the present study are mainly qualitative in this regard, they indicate that future analysis of quantitative relationships between thunderstorm characteristics (e.g., echo volume/area, convective/stratiform fractions, and total flash rate) and large-CMC lightning could be fruitful if applied to a larger climatological data set. The CMCN in the United States has been in operation since 2007 [Cummer *et al.*, 2013; Beavis *et al.*, 2014], making such an analysis realistic. This could lead to new applications for the CMC metric in diagnosing the characteristics and evolution of storms. In other words, charge moment change should not be considered a niche metric suitable only for TLE and upper atmospheric research. It has potential applications for studying tropospheric weather.

References

- Beavis, N., T. J. Lang, S. A. Rutledge, W. A. Lyons, and S. A. Cummer (2014), Diurnal, seasonal, and regional behavior of cloud-to-ground lightning with large impulse charge moment changes, *Mon. Weather Rev.*, doi:10.1175/MWR-D-14-00034.1.
- Biagi, C. J., K. L. Cummins, K. E. Kehoe, and E. P. Krider (2007), National Lightning Detection Network (NLDN) performance in southern Arizona, Texas, and Oklahoma in 2003–2004, *J. Geophys. Res.*, *112*, D05208, doi:10.1029/2006JD007341.
- Boccippio, D. J., E. R. Williams, W. A. Lyons, I. Baker, and R. Boldi (1995), Sprites, ELF transients and positive ground strokes, *Science*, *269*, 1088–1091.
- Browning, K. A. (1964), Airflow and precipitation trajectories within severe local storms which travel to the right of the winds, *J. Atmos. Sci.*, *21*, 634–639.
- Bruning, E. C., and D. R. MacGorman (2013), Theory and observations of controls on lightning flash size spectra, *J. Atmos. Sci.*, *70*, 4012–4029.
- Bruning, E. C., W. D. Rust, D. R. MacGorman, M. I. Biggerstaff, and T. J. Schuur (2010), Formation of charge structures in a supercell, *Mon. Weather Rev.*, *138*, 3740–3761.
- Bruning, E. C., S. A. Weiss, and K. M. Calhoun (2014), Continuous variability in thunderstorm primary electrification and an evaluation of inverted-polarity terminology, *Atmos. Res.*, *136*, 274–284.
- Carey, L. D., and S. A. Rutledge (1998), Electrical and multiparameter radar observations of a severe hailstorm, *J. Geophys. Res.*, *103*(D12), 13,979–14,000, doi:10.1029/97JD02626.
- Carey, L. D., M. J. Murphy, T. L. McCormick, and N. W. S. Demetriades (2005), Lightning location relative to storm structure in a leading-line, trailing-stratiform mesoscale convective system, *J. Geophys. Res.*, *110*, D03105, doi:10.1029/2003JD004371.
- Cummer, S. A., and U. S. Inan (2000), Modeling ELF radio atmospheric propagation and extracting lightning currents from ELF observations, *Radio Sci.*, *35*(2), 385–394, doi:10.1029/1999RS002184.
- Cummer, S. A., and W. A. Lyons (2004), Lightning charge moment changes in U.S. High Plains thunderstorms, *Geophys. Res. Lett.*, *31*, L05114, doi:10.1029/2003GL019043.
- Cummer, S. A., and W. A. Lyons (2005), Implications of lightning charge moment changes for sprite initiation, *J. Geophys. Res.*, *110*, A04304, doi:10.1029/2004JA010812.
- Cummer, S. A., W. A. Lyons, and M. A. Stanley (2013), Three years of lightning impulse charge moment change measurements in the United States, *J. Geophys. Res. Atmos.*, *118*, 5176–5189, doi:10.1002/jgrd.50442.
- Cummins, K. L., and M. J. Murphy (2009), An overview of lightning location systems: History, techniques, and data uses, with an in-depth look at the U.S. NLDN, *IEEE Trans. Electromagn. Compat.*, *51*(3), 499–518.
- Cummins, K. L., M. J. Murphy, E. A. Bardo, W. L. Hiscox, R. B. Pyle, and A. E. Pifer (1998), A combined TOA/MDF technology upgrade of the U.S. National Lightning Detection Network, *J. Geophys. Res.*, *103*, 9035–9044, doi:10.1029/98JD00153.

Acknowledgments

This research is dedicated in memory of Tim Samaras, his son Paul, and his colleague Carl Young, all of whom lost their lives in the El Reno tornado. Tim Samaras was a valuable collaborator on the Physical Origins of Coupling to the upper Atmosphere from Lightning (PhOCAL) project, and his contributions are greatly missed. The research presented here is part of PhOCAL, which is led by Duke University and funded by the Defense Advanced Research Projects Agency via the Nimbus program. Flores-Rivera's work on this case was supported by the NASA Marshall summer 2013 internship program and the NASA Lightning Imaging Sensor project. The authors gratefully acknowledge the valuable contributions of the NLDN data from Vaisala, Inc., which enables the geolocation of large-CMC events by the CMCN. NLDN data are available commercially from Vaisala (<http://www.vaisala.com/en/products/thunderstormandlightningdetection-systems/Pages/NLDN.aspx>). CMCN data are available upon request from co-author Steve Cummer (cummer@ee.duke.edu). OKLMA data are available upon request from co-authors Don MacGorman (don.macgorman@noaa.gov) or William Beasley (whb@ou.edu). MRMS mosaics are available from NSSL (<http://www.nssl.noaa.gov>). All IDL and Python scripts used to perform the analyses and create the plots in this report are available upon request from lead author Timothy Lang (timothy.j.lang@nasa.gov). IDL is available for purchase from <http://www.exelisvis.com/ProductsServices/IDL.aspx>. A free distribution of Python may be obtained from <https://store.continuum.io/cshop/anaconda/>. The views, opinions, and findings in this report are those of the authors and should not be construed as an official NASA, NOAA, or U.S. Government position, policy, or decision.

- Darden, C. B., D. J. Nadler, B. C. Carcione, R. J. Blakeslee, G. T. Stano, and D. E. Buechler (2010), Utilizing total lightning information to diagnose convective trends, *Bull. Am. Meteorol. Soc.*, *91*, 167–175.
- Ely, B. L., R. E. Orville, L. D. Carey, and C. L. Hodapp (2008), Evolution of the total lightning structure in a leading-line, trailing-stratiform mesoscale convective system over Houston, Texas, *J. Geophys. Res.*, *113*, D08114, doi:10.1029/2007JD008445.
- Emeric, C., P. L. Heinselman, D. R. MacGorman, and E. C. Bruning (2011), Lightning activity in a hail-producing storm observed with phased-array radar, *Mon. Weather Rev.*, *139*, 1809–1825.
- Gatlin, P. N., and S. J. Goodman (2010), A total lightning trending algorithm to identify severe thunderstorms, *J. Atmos. Oceanic Technol.*, *27*, 3–22.
- Goodman, S. J., et al. (2005), The North Alabama Lightning Mapping Array: Recent severe storm observations and future prospects, *Atmos. Res.*, *76*, 423–437, doi:10.1016/j.atmosres.2004.11.035.
- Hu, W., S. A. Cummer, W. A. Lyons, and T. E. Nelson (2002), Lightning charge moment changes for the initiation of sprites, *Geophys. Res. Lett.*, *29*(8), 1279, doi:10.1029/2001GL014593.
- Huang, E., E. Williams, R. Boldi, S. Heckman, W. Lyons, M. Taylor, T. Nelson, and C. Wong (1999), Criteria for sprites and elves based on Schumann resonance observation, *J. Geophys. Res.*, *104*(D14), 16,943–16,964, doi:10.1029/1999JD900139.
- Istok, M. J., and R. J. Doviak (1986), Analysis of the relation between Doppler spectral width and thunderstorm turbulence, *J. Atmos. Sci.*, *43*, 2199–2214.
- Koshak, W. J., et al. (2004), North Alabama Lightning Mapping Array (LMA): VHF source retrieval algorithm and error analyses, *J. Atmos. Oceanic Technol.*, *21*, 543–558.
- Krehbiel, P. R., R. J. Thomas, W. Rison, T. Hamlin, J. Harlin, and M. Davis (2000), GPS-based mapping system reveals lightning inside storms, *Eos Trans., AGU*, *81*, 21–25.
- Krehbiel, P. R., J. A. Rioussel, V. P. Pasko, R. J. Thomas, W. Rison, M. A. Stanley, and H. E. Edens (2008), Upward electrical discharges from thunderstorms, *Nat. Geosci.*, *1*, 233–237, doi:10.1038/ngeo162.
- Lang, T. J., and S. A. Rutledge (2008), Kinematic, microphysical, and electrical aspects of an asymmetric bow-echo mesoscale convective system observed during STEPS 2000, *J. Geophys. Res.*, *113*, D08213, doi:10.1029/2006JD007709.
- Lang, T. J., and S. A. Rutledge (2011), A framework for the statistical analysis of large radar and lightning data sets: Results from STEPS 2000, *Mon. Weather Rev.*, *139*, 2536–2551.
- Lang, T. J., et al. (2004a), The Severe Thunderstorm Electrification and Precipitation Study, *Bull. Am. Meteorol. Soc.*, *85*, 1107–1125.
- Lang, T. J., S. A. Rutledge, and K. C. Wiens (2004b), Origins of positive cloud-to-ground lightning flashes in the stratiform region of a mesoscale convective system, *Geophys. Res. Lett.*, *31*, L10105, doi:10.1029/2004GL019823.
- Lang, T. J., W. A. Lyons, S. A. Rutledge, J. D. Meyer, D. R. MacGorman, and S. A. Cummer (2010), Transient luminous events above two mesoscale convective systems: Storm structure and evolution, *J. Geophys. Res.*, *115*, A00E22, doi:10.1029/2009JA014500.
- Lang, T. J., J. Li, W. A. Lyons, S. A. Cummer, S. A. Rutledge, and D. R. MacGorman (2011), Transient luminous events above two mesoscale convective systems: Charge moment change analysis, *J. Geophys. Res.*, *116*, A10306, doi:10.1029/2011JA016758.
- Lang, T. J., S. A. Cummer, S. A. Rutledge, and W. A. Lyons (2013), The meteorology of negative cloud-to-ground lightning strokes with large charge moment changes: Implications for negative sprites, *J. Geophys. Res. Atmos.*, *118*, 7886–7896, doi:10.1002/jgrd.50595.
- Lu, G., S. A. Cummer, R. J. Blakeslee, S. Weiss, and W. H. Beasley (2012), Lightning morphology and impulse charge moment change of high peak current negative strokes, *J. Geophys. Res.*, *117*, D04212, doi:10.1029/2011JD016890.
- Lu, G., et al. (2013), Coordinated observations of sprites and in-cloud lightning flash structure, *J. Geophys. Res. Atmos.*, *118*, 6607–6632, doi:10.1002/jgrd.50459.
- Lyons, W. A. (1996), Sprite observations above the U.S. High Plains in relation to their parent thunderstorm systems, *J. Geophys. Res.*, *101*, 29,641–29,652, doi:10.1029/96JD01866.
- Lyons, W. A. (2006), The meteorology of transient luminous events: An introduction and overview, in *NATO Advanced Study Institute on Sprites, Elves and Intense Lightning Discharges*, edited by M. Fullekrug et al., pp. 19–56, Springer, Dordrecht, Netherlands.
- Lyons, W. A., T. E. Nelson, E. R. Williams, S. A. Cummer, and M. A. Stanley (2003), Characteristics of sprite-producing positive cloud-to-ground lightning during the 19 July 2000 STEPS mesoscale convective systems, *Mon. Weather Rev.*, *131*, 2417–2427.
- Lyons, W. A., S. A. Cummer, M. A. Stanley, G. R. Huffines, K. C. Wiens, and T. E. Nelson (2008), Supercells and sprites, *Bull. Am. Meteorol. Soc.*, *89*, 1165–1174.
- Lyons, W. A., M. Stanley, J. D. Meyer, T. E. Nelson, S. A. Rutledge, T. J. Lang, and S. A. Cummer (2009), The meteorological and electrical structure of TLE-producing convective storms, in *Lightning: Principles, Instruments and Applications*, edited by H. D. Betz et al., pp. 389–417, Springer Science+Business Media B.V., Dordrecht, Netherlands, doi:10.1007/978-1-4020-9079-0_17.
- MacGorman, D. R., et al. (2008), TELEX: The Thunderstorm Electrification and Lightning Experiment, *Bull. Am. Meteorol. Soc.*, *89*, 997–1013.
- Meyer, T. C., T. J. Lang, S. A. Rutledge, W. A. Lyons, S. A. Cummer, G. Lu, and D. T. Lindsey (2013), Radar and lightning analyses of gigantic jet-producing storms, *J. Geophys. Res. Atmos.*, *118*, 2872–2888, doi:10.1002/jgrd.50302.
- Pasko, V. P. (2010), Recent advances in theory of transient luminous events, *J. Geophys. Res.*, *115*, A00E35, doi:10.1029/2009JA014860.
- Potter, S. (2007), Fine-Tuning Fujita: After 35 years, a new scale for rating tornadoes takes effect, *Weatherwise*, *60*, 64–71.
- Qin, J., S. J. Celestin, and V. P. Pasko (2012), Minimum charge moment change in positive and negative cloud to ground lightning discharges producing sprites, *Geophys. Res. Lett.*, *39*, L22801, doi:10.1029/2012GL053951.
- Rison, W., R. J. Thomas, P. R. Krehbiel, T. Hamlin, and J. Harlin (1999), A GPS-based three-dimensional lightning mapping system: Initial observations in central New Mexico, *Geophys. Res. Lett.*, *26*, 3573–3576, doi:10.1029/1999GL010856.
- São Sabbas, F. T., and D. D. Sentman (2003), Dynamical relationship of infrared cloudtop temperatures with occurrence rates of cloud-to-ground lightning and sprites, *Geophys. Res. Lett.*, *30*(51236), doi:10.1029/2002GL015382.
- Schultz, C. J., W. A. Petersen, and L. D. Carey (2009), Preliminary development and evaluation of lightning jump algorithms for the real-time detection of severe weather, *J. Appl. Meteorol. Climatol.*, *48*, 2543–2563.
- Schultz, C. J., W. A. Petersen, and L. D. Carey (2011), Lightning and severe weather: A comparison between total and cloud-to-ground lightning trends, *Weather Forecasting*, *26*, 744–755.
- Soula, S., O. van der Velde, J. Montanya, T. Neubert, O. Chanrion, and M. Ganot (2009), Analysis of thunderstorm and lightning activity associated with sprites observed during the EuroSprite campaigns: Two case studies, *Atmos. Res.*, *91*(2–4), 514–528, doi:10.1016/j.atmosres.2008.06.017.
- Soula, S., F. Iacovella, O. van der Velde, J. Montanya, M. Füllekrug, T. Farges, J. Bór, J.-F. Georgis, S. NaitAmor, and J.-M. Martin (2014), Multi-instrumental analysis of large sprite events and their producing storm in southern France, *Atmos. Res.*, *136*, 415–431.
- Stolzenburg, M., W. D. Rust, and T. C. Marshall (1998), Electrical structure in thunderstorm convective regions: 2. Isolated storms, *J. Geophys. Res.*, *103*(D12), 14,079–14,096, doi:10.1029/97JD03547.

- Thomas, R. J., P. R. Krehbiel, W. Rison, S. J. Hunyady, W. P. Winn, T. Hamlin, and J. Harlin (2004), Accuracy of the Lightning Mapping Array, *J. Geophys. Res.*, *109*, D14207, doi:10.1029/2004JD004549.
- van der Velde, O. A., and J. Montanyà (2013), Asymmetries in bidirectional leader development of lightning flashes, *J. Geophys. Res. Atmos.*, *118*, 13,504–13,519, doi:10.1002/2013JD020257.
- van der Velde, O. A., J. Montanyà, S. Soula, N. Pineda, and J. Mlynarczyk (2014), Bidirectional leader development in sprite-producing positive cloud-to-ground flashes: Origins and characteristics of positive and negative leaders, *J. Geophys. Res. Atmos.*, *119*, 12,755–12,779, doi:10.1002/2013JD021291.
- Wiens, K. C., S. A. Rutledge, and S. A. Tessendorf (2005), The 29 June 2000 supercell observed during STEPS. Part II: Lightning and charge structure, *J. Atmos. Sci.*, *62*, 4151–4177.
- Williams, E. R. (2001), The electrification of severe storms, in *Severe Convective Storms*, Meteorol. Monogr., vol. 49, pp. 527–561, Am. Meteorol. Soc., Boston, Mass.
- Williams, E. R., and Y. Yair (2006), The microphysical and electrical properties of sprite-producing thunderstorms, in *NATO Advanced Study Institute on Sprites, Elves and Intense Lightning Discharges*, edited by M. Fullekrug et al., pp. 57–83, Springer, Dordrecht, Netherlands.
- Williams, E., B. Boldi, A. Matlin, M. Weber, S. Hodanish, D. Sharp, S. Goodman, R. Raghavan, and D. Buechler (1999), The behavior of total lightning activity in severe Florida thunderstorms, *Atmos. Res.*, *51*, 245–265.
- Wurman, J., K. Kosiba, P. Robinson, and T. Marshall (2014), The role of multiple-vortex tornado structure in causing storm researcher fatalities, *Bull. Am. Meteorol. Soc.*, *95*, 31–45.
- Zhang, J., et al. (2011), National Mosaic and Multi-Sensor QPE (NMQ) System: Description, results, and future plans, *Bull. Am. Meteorol. Soc.*, *92*, 1321–1338.